

Turbulence and its parameterization in accretion discs

AXEL BRANDENBURG

NORDITA, Blegdamsvej 17, DK-2100 Copenhagen Ø, Denmark

Received 8 September 2005; accepted 22 September 2005; published online 20 October 2005

Abstract. Accretion disc turbulence is investigated in the framework of the shearing box approximation. The turbulence is either driven by the magneto-rotational instability or, in the non-magnetic case, by an explicit and artificial forcing term in the momentum equation. Unlike the magnetic case, where most of the dissipation occurs in the disc corona, in the forced hydrodynamic case most of the dissipation occurs near the midplane. In the hydrodynamic case evidence is presented for the stochastic excitation of epicycles. When the vertical and radial epicyclic frequencies are different (modeling the properties around rotating black holes), the beat frequency between these two frequencies appear to show up as a peak in the temporal power spectrum in some cases. Finally, the full turbulent resistivity tensor is determined and it is found that, if the turbulence is driven by a forcing term, the signs of its off-diagonal components are such that this effect would not be capable of dynamo action by the shear-current effect.

Key words: Accretion, accretion discs – Magnetohydrodynamics (MHD) – Turbulence

©0000 WILEY-VCH Verlag GmbH & Co. KGaA, Weinheim

1. Introduction

It is now generally accepted that angular momentum transport in accretion discs is accomplished by hydromagnetic turbulence that is produced by the magneto-rotational instability (MRI, also known as Balbus-Hawley instability); see Balbus & Hawley (1991, 1998). The significance of this mechanism for accretion discs has been established using local shearing box simulations (Hawley et al. 1995, 1996, Matsumoto & Tajima 1995, Brandenburg et al. 1995, 1996a, Stone et al. 1996), as well as global simulations (Hawley 2000, Arlt & Rüdiger 2001, De Villiers & Hawley 2003). For many purposes one would like to parameterize the turbulence in terms of a turbulent viscosity. The ultimate goal of such an approach is to be able to capture the relevant pieces of turbulence physics in two-dimensional axisymmetric and one-dimensional vertically integrated models of accretion discs. Even if this turns out not to be possible, parameterized models are still extremely useful for illuminating otherwise unrecognized mechanisms that might only be directly identifiable using a targeted approach.

One aspect that we do not understand very well right now is to what extent MRI-driven turbulence is similar to ordinary (e.g. forced) turbulence. This question is relevant because one is tempted to apply some well-known turbulence concepts quite loosely also to MRI-driven turbulence without distin-

guishing between the different forms of driving. In order to address this question we consider here the case of forced turbulence and compare with what has been found for MRI-driven turbulence. In addition to the forced simulations we also present solutions of MRI-driven turbulence that have not previously been published. No net magnetic flux is imposed, so we are able to have a self-sustained mechanism. Most previous approaches used numerical viscosity and resistivity. With the regular laplacian diffusion operator (proportional to ∇^2) self-sustained turbulence is only possible at large resolution (more than 128^3 meshpoints; see Brandenburg et al. 2004). This becomes prohibitively expensive if we need to achieve sufficient statistics and long enough runs. Therefore, we adopt hyperdiffusion for these runs (here proportional to ∇^6), analogous to what was done also in Brandenburg et al. (1995). All forced simulations are however done with regular laplacian diffusion.

One of the goals of this paper is to reconsider the numerical determination of turbulent viscosity and resistivity in local simulations of accretion flows. This is motivated by recent advances in the case of non-shearing and non-rotating flows. Particular attention is paid to the tensorial nature of the turbulent resistivity tensor and the differences between forced and MRI-driven turbulence. For the turbulent viscosity the tensorial nature is important for modeling warps in accretion discs (Torkelsson et al. 2000). This has also motivated the study of

the tensorial nature of turbulent passive scalar diffusion (Carballido et al. 2005, Johansen & Klahr 2005).

In the following we use overbars to denote spatial averages over one or two coordinate directions, e.g. azimuthal averages and occasionally also vertical averages. Angular brackets without subscript are used for volume averages, while angular brackets with subscript t denote time averages.

2. Stress and strain

In any parameterized model of a turbulent flow one is interested in the Reynolds stress $\overline{\rho u_i u_j}$ and, if magnetic fields are present, in the Maxwell stress $\frac{1}{2} \delta_{ij} \overline{b^2} - \overline{b_i b_j}$. Here, the magnetic field is measured in units where the vacuum permeability is unity, and lower case characters \mathbf{u} and \mathbf{b} denote deviations from the mean flow $\overline{\mathbf{U}}$ and the mean field $\overline{\mathbf{B}}$, so $\overline{\mathbf{U}} = \mathbf{U} + \mathbf{u}$ and $\overline{\mathbf{B}} = \mathbf{B} + \mathbf{b}$ are the full velocity and magnetic fields. So the full turbulent stress from the small scales (SS) is given by

$$\overline{\Pi}_{ij}^{(SS)} = \overline{\rho u_i u_j} + \frac{1}{2} \delta_{ij} \overline{b^2} - \overline{b_i b_j}. \quad (1)$$

Analogously, one can define the total stress from the large scale (LS) fields,

$$\overline{\Pi}_{ij}^{(LS)} = \rho \overline{U_i U_j} + \frac{1}{2} \delta_{ij} \overline{B^2} - \overline{B_i B_j}. \quad (2)$$

In the steady state, the value of the turbulent mass accretion rate, for example, follows from the constancy of the angular momentum flux, i.e.

$$\int_0^{2\pi} \varpi d\phi \int_{-h}^h dz \left(\overline{\Pi}_{\varpi\phi}^{(LS)} + \overline{\Pi}_{\varpi\phi}^{(SS)} \right) = C \equiv \text{const}, \quad (3)$$

where we have neglected the microscopic viscosity, because it is very small in discs (although not necessarily in simulations!). Here, cylindrical polar coordinates, (ϖ, ϕ, z) , have been employed, and h denotes the disc height (e.g. its gaussian scale height). In Eq. (3) we can isolate the mass accretion rate, $\dot{M} = - \int \varpi d\phi \int dz \rho \overline{U}_\varpi$. Replacing furthermore the integration by a multiplication with $4\pi\varpi h$, we find

$$\dot{M} = \frac{4\pi h}{\overline{\omega U}_\phi} \left(\overline{\varpi \Pi}_{\varpi\phi}^{(LS)} - \overline{\varpi B}_\varpi \overline{B}_\phi - C \right). \quad (4)$$

Remarkably, for calculating the accretion rate it suffices to know only the value of the stress, not its functional dependence on the mean flow properties. The same is true of the heating rate, which is given by (e.g., Balbus & Papaloizou 1999, Balbus 2004)

$$\dot{E} = 4\pi h \left(\overline{\varpi \frac{\partial \overline{\Omega}}{\partial \varpi}} \right) \left(\overline{\Pi}_{\varpi\phi}^{(LS)} + \overline{\Pi}_{\varpi\phi}^{(SS)} \right), \quad (5)$$

where $\overline{\Omega} = \overline{U}_\phi / \varpi$ has been introduced, and only the shear from the differential rotation has been taken into account.

However, for many (if not all) other purposes it is necessary to know also the functional dependence of the stress on other quantities, most notably the shear rate. In fact, a common proposal is to approximate the mean stress by the mean rate-of-strain tensor \overline{S}_{ij} and to write

$$\overline{\Pi}_{ij}^{(SS)} \approx 2\rho\nu_t \overline{S}_{ij}, \quad (6)$$

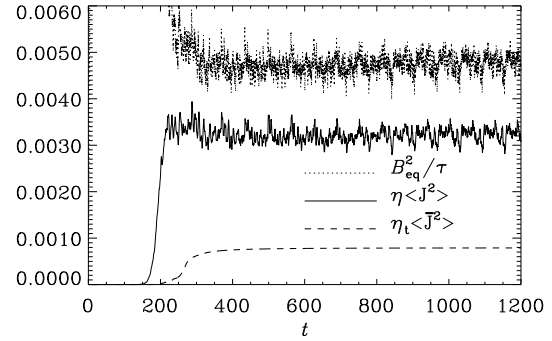


Fig. 1. Joule dissipation for Run 3 of Brandenburg (2001, solid line), compared with the Joule dissipation estimated for a corresponding mean-field model (dashed line). An estimate for the rate of total energy dissipation, B_{eq}^2/τ , is also given. [Adapted from Brandenburg (2003).]

where $\overline{S}_{ij} = \frac{1}{2}(\overline{U}_{i,j} + \overline{U}_{j,i})$ is the rate of strain of the mean flow, and ν_t is a turbulent transport coefficient (turbulent viscosity).¹

The significance of Eq. (6) is that it provides a closure for the small scale quantity $\overline{\Pi}_{ij}^{(SS)}$ in terms of the large scale strain, \overline{S}_{ij} . This is, unlike the previous relations in this section, necessarily only an approximation. In the equation of angular momentum conservation this term acts as a diffusion term and provides angular momentum transport in the direction of decreasing angular velocity, i.e. outward.

As we discussed above, the stress also contributes to the rate of heating of the disc. The horizontally averaged rate of viscous heating (per unit volume) is given by

$$Q_{\text{visc}} = 2\rho\nu \overline{\mathbf{S}^2} \quad (\text{actual heating rate}), \quad (7)$$

where \mathbf{S} is the actual rate of strain matrix, is assumed to be approximated by

$$Q_{\text{visc}} \approx 2\rho\nu_t \overline{\mathbf{S}^2} \quad (\text{parameterized heating rate}), \quad (8)$$

where $\overline{\mathbf{S}}$ is the rate of strain of the mean flow. [In accretion discs, where keplerian shear gives the largest contribution to $\overline{\mathbf{S}^2}$, Eq. (8) yields the familiar expression $Q_{\text{visc}} \approx \rho\nu_t (\frac{3}{2}\overline{\Omega})^2$; see Frank et al. (1992).] Of course, $\overline{\mathbf{S}^2} \gg \overline{\mathbf{S}}^2$ and $\nu_t \gg \nu$, but whether $\nu_t \overline{\mathbf{S}^2}$ is actually the same as $\nu \overline{\mathbf{S}^2}$ is not obvious.

Using the first order smoothing approximation, which is commonly used in mean field dynamo theory, Rüdiger (1987) found that $\nu \overline{\mathbf{S}^2}$ is actually about 3 times larger than what is expected from $\nu_t \overline{\mathbf{S}^2}$. It is still unclear whether this is actually true, or whether it is an artifact of the first order smoothing approximation and that the two expressions should really be the same.

In quite a different context of hydromagnetic turbulence, where a helical large scale mean field is generated (so that the

¹ The mean flow is here solenoidal, so \overline{S}_{ij} is trace-less. In the general case considered below an extra term is added to make sure S_{ij} is trace-free.

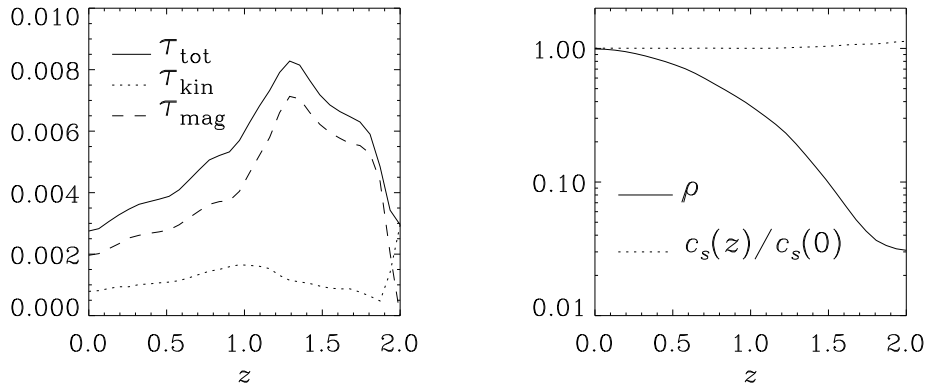


Fig. 2. Dependence of the stress component $\overline{\Pi}_{\omega\phi}^{(SS)}$ (here denoted by τ_{xy}), separately for the kinetic and magnetic contributions, together with the sum of the two denoted by total (left) as well as the vertical dependence of density and sound speed (right). Note that τ_{xy} is neither proportional to the density ρ nor the sound speed c_s . [Adapted from Brandenburg et al. (1996b).]

mean current density is well defined), an equivalent conclusion was reached for the actual and parameterized *resistive* heating rates, i.e.

$$\overline{\eta \mathbf{J}^2} \approx 3.7 \times \eta_t \overline{\mathbf{J}^2}, \quad (9)$$

see Brandenburg (2003) and Fig. 1 where we also compare with an estimate for the rate of total energy dissipation, B_{eq}^2/τ , where τ is the turnover time. Here we have used for η_t the value estimated from the self-consistently determined empirical quenching formula of Brandenburg (2001) for his Run 3. The factor 3.7 in Eq. (9) is similar to what has been found for the turbulent viscosity (Rüdiger 1987). This suggests that his result obtained within the framework of the first order smoothing approximation is at least not in conflict with the simulations.

We now turn to another aspect of viscous heating. In MRI-driven turbulence it was found that the stress does not decrease with height away from the midplane, as suggested by Eq. (6), even though the product of rate of strain and density does decrease because of decreasing density. This was originally demonstrated only for nearly isothermal discs (Brandenburg et al. 1996b), see Fig. 2, but this has now also been shown for radiating discs (Turner 2004).

Indeed, it was found that ρ should rather be replaced by the vertically averaged density. A sensible parameterization seemed therefore only possible for the vertically integrated stress, i.e. (Brandenburg et al. 1996b)

$$\int_{-h}^h dz \overline{\Pi}_{\omega\phi}^{(SS)} \approx \alpha_{SS} \int_{-h}^h dz \rho c_s^2, \quad (10)$$

where α_{SS} is the dimensionless Shakura-Sunyaev (1973) viscosity coefficient and c_s is the sound speed. The reason for this is quite clearly related to the fact that the stress is of magnetic origin, and that most of the dissipation happens when the density is low, i.e. when the ohmic heating rate per unit mass, $\mathbf{J}^2/(\sigma\rho)$, is large (here, \mathbf{J} is the current density, and σ the electric conductivity). However, it would be surprising if the absence of a scaling of the stress with the density were a general property.

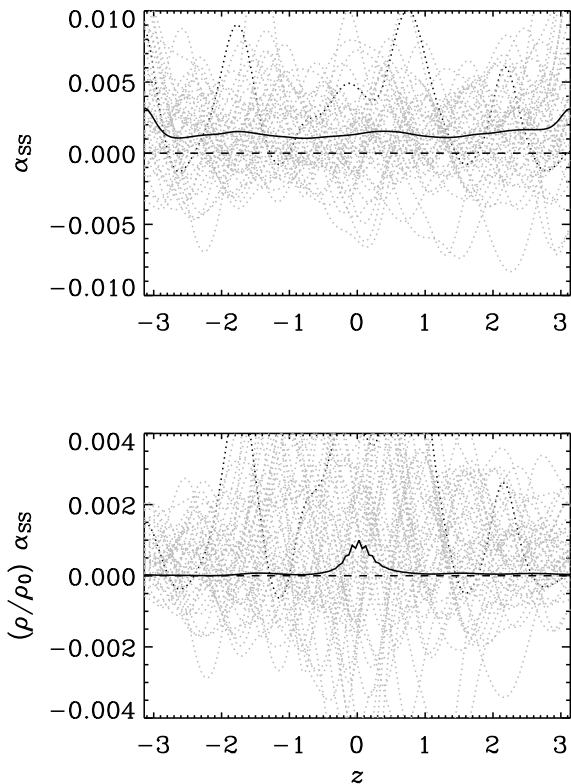


Fig. 3. Vertical dependence of α_{SS} for hydrodynamic forced shear flow turbulence (upper panel). The solid curves give the time average while a few individual times are plotted in gray. Note that the temporal average of α_{SS} is nearly constant in z , although for individual times there can be significant fluctuations. By comparison, the density-weighted viscosity parameter decreases with height (lower panel), showing that in forced non-magnetic turbulence the stress is indeed proportional to the density.

In order to shed some light on this question we now consider a hydrodynamic shearing box model where the turbulence is driven by an explicit body force that is delta-

correlated in time and monochromatic in space with a wavenumber of $k_f \approx 3$. (Details of this simulation are given in Sect. 3.) The result is shown in Fig. 3, where we have expressed the result in terms of a vertically dependent Shakura-Sunyaev viscosity coefficient $\alpha_{SS}(z)$, so

$$\nu_t(z) = \alpha_{SS}(z) c_s h. \quad (11)$$

Note that in the present case of purely hydrodynamic forced turbulence $\alpha_{SS}(z)$ is nearly independent of height, even though ρ varies by at least an order of magnitude, as can be seen from the second panel of Fig. 3, where we show the product $\rho(z)\alpha_{SS}(z)$, normalized by the initial density in the midplane, ρ_0 .

In the following section we reiterate the standard shearing box equation that have been used to obtain this result.

3. Shearing box equations

We consider here a domain of size $L_x \times L_y \times L_z$, where $L_x = L_y = 2\pi$ and $L_z = 4$, although other choices are possible and have been considered in the earlier work. We solve the equations for the departure from the keplerian shear flow for an isothermal equation of state (so the pressure is given by $p = \rho c_s^2$). The resulting equations can be written in the form

$$\frac{Du_i}{Dt} = -u_j \frac{\partial \bar{U}_i}{\partial x_j} + \left(\frac{\mathbf{J} \times \mathbf{B}}{\rho} - c_s^2 \nabla \ln \rho - 2\Omega \times \mathbf{u} \right)_i - \zeta^2 z_i + f_i + \nu \left(\nabla^2 u_i + \frac{1}{3} \frac{\partial}{\partial x_i} \nabla \cdot \mathbf{u} + 2S_{ij} \frac{\partial \ln \rho}{\partial x_j} \right), \quad (12)$$

$$\frac{DA_i}{Dt} = -A_j \left(\frac{\partial \bar{U}_j}{\partial x_i} + \frac{\partial u_j}{\partial x_i} \right) + \eta \nabla^2 A_i, \quad (13)$$

$$\frac{D \ln \rho}{Dt} = -\nabla \cdot \mathbf{u}, \quad (14)$$

where $D/Dt = \partial/\partial t + (\bar{\mathbf{U}} + \mathbf{u}) \cdot \nabla$ is the advective derivative based on the full flow field that includes both the shear flow and the deviations from it. We solve the equations for the departure, \mathbf{u} , from the purely linear shear flow. Except for the advection operator, only derivatives of $\bar{\mathbf{U}}$ enter. This is an important property of the shearing sheet approximation that is critical for being able to use shearing-periodic boundary conditions in the x direction. We have used the gauge

$$\phi = \eta \nabla \cdot \mathbf{A} - (\bar{\mathbf{U}} + \mathbf{u}) \cdot \mathbf{A}, \quad (\text{assuming } \eta = \text{const}). \quad (15)$$

for the electrostatic potential. The shear flow is given by $\bar{\mathbf{U}}(x) = (0, -q\Omega x, 0)$, where $q = 3/2$ for a purely keplerian shear flow, and

$$S_{ij} = \frac{1}{2} \left(\frac{\partial u_i}{\partial x_j} + \frac{\partial u_j}{\partial x_i} \right) - \frac{1}{3} \delta_{ij} \nabla \cdot \mathbf{u} \quad (16)$$

is the traceless rate of strain matrix. The Coriolis force is added to take into account that the shearing box is spinning about the central star at angular velocity Ω . This together with shear can lead to radial epicyclic oscillations with frequency $\kappa = \sqrt{2(2-q)}\Omega$. (17)

Note that $\kappa = \Omega$ for a keplerian disc with $q = 3/2$. The term $-\zeta^2 \hat{z}$ characterizes the vertical stratification, where ζ is

the vertical epicyclic frequency. Again, in a keplerian disc we have $\zeta = \Omega$, but here we treat ζ as an independent parameter in order to assess the effects of different radial and vertical epicyclic frequencies in non-newtonian discs with different radial and vertical epicyclic frequencies (Abramowicz et al. 2003a,b, Kato 2004, Kluźniak et al. 2004, Lee et al. 2004). For most of the cases considered below we choose $\Omega = \kappa = 0.4$ and $\zeta = 0.6$. The sound speed is taken to be $c_s = 1$. (With these parameters the magnitude of the shear flow is $\frac{3}{2}\Omega(L_x/2) \approx 1.9$, so it is weakly supersonic.) In the nonmagnetic cases ($\mathbf{A} = 0$) we allow for the possibility of an extra forcing term \mathbf{f} in order to study the case of non-magnetic (non-MRI) turbulence. The forcing function is identical to that used by Brandenburg (2001) for forced turbulent simulations exhibiting dynamo action. The amplitude of the forcing function is denoted by f_0 which is here chosen to be 0.01, unless it put to zero. The details of this forcing function are summarized in Appendix A.

The boundary conditions adopted in the vertical direction on $z = \pm L_z/2$ are

$$u_{x,z} = u_{y,z} = u_z = A_x = A_y = A_{z,z} = 0, \quad (18)$$

which corresponds to a perfect conductor no-slip condition. Here, commas denote partial differentiation.

The results presented here have been obtained with the PENCIL CODE,² which is a public domain code for solving the compressible hydromagnetic (and other) equations on massively parallel distributed memory architectures such as Beowulf clusters. It employs a high-order finite-difference scheme (sixth order in space and third order in time), which is ideal for all types of turbulence simulations.

The present simulations are mainly exploratory in nature, so we only use small to moderate resolution between 32^3 and 128^3 meshpoints. Restrictions in resolution are also imposed by the need to run for long enough times in order to overcome transients.

4. Growth and decay of epicycles

One way of estimating the effective viscosity of a system is to determine the decay rate of a velocity perturbation that has initially a sinusoidal variation in one spatial direction. As an example one may consider an initial mean velocity perturbation of the form

$$\mathbf{u}(\mathbf{x}, 0) = \bar{\mathbf{U}}_0(0) \sin \mathbf{k}_i \cdot \mathbf{x} \quad (19)$$

for different directions i of the wavevector \mathbf{k}_i . The time dependence of the amplitude $\bar{\mathbf{U}}_0(t)$ can be determined by projecting on the original velocity, i.e.

$$\bar{\mathbf{U}}_0(t) = 2 \langle \bar{\mathbf{U}}(\mathbf{x}, t) \sin \mathbf{k}_i \cdot \mathbf{x} \rangle, \quad (20)$$

where the angular brackets denote volume averaging. The effective viscosity is connected with the decay rate λ via $\lambda = \nu_t \mathbf{k}_i$, and λ is measured as

$$\lambda = -\langle d \ln |\bar{\mathbf{U}}_0(t)| / dt \rangle_t, \quad (21)$$

where $\langle \cdot \rangle_t$ denotes a time average over a suitable time interval when the decay is exponential. In forced turbulence it was found that $\nu_t \approx (0.8 \dots 0.9) \times u_{\text{rms}}/k_f$ (Yousef et al. 2003).

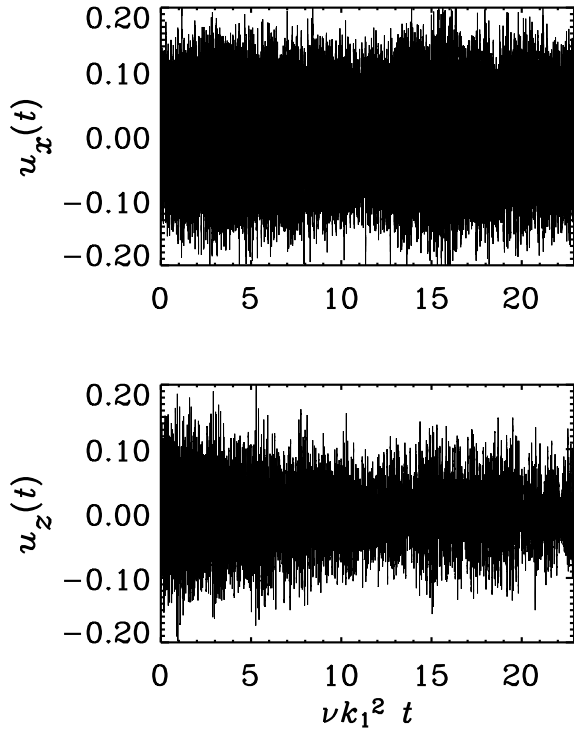


Fig. 4. Time dependence of the vertical and radial velocity components at one point. Note that time is represented in viscous units, where $2\pi/k_1$ is the vertical extent of the computational domain. Evidently, the decay of the vertical epicyclic oscillations in u_z is very small (lower panel), and there is no decay of u_x (upper panel).

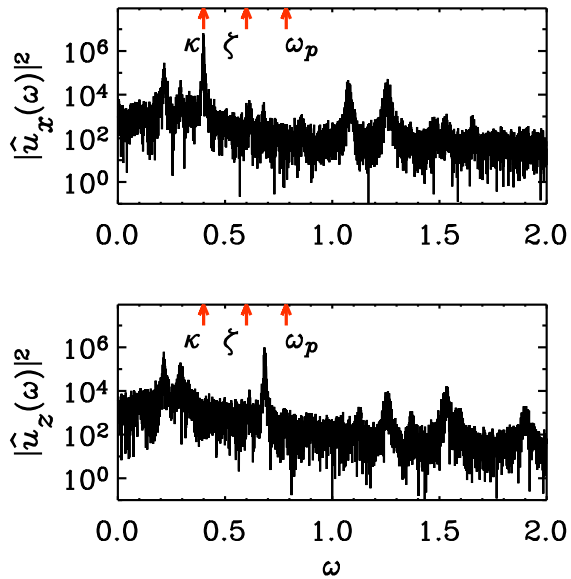


Fig. 5. Power spectra of u_x and u_z . The orbit of the initial state is perturbed, using $\mathbf{u} = (0.1, 0, 0.1)$, such that radial and vertical epicyclic motions are excited with frequencies $\kappa = \Omega = 0.4$ and $\zeta = 0.6$ (marked by arrows in the two diagrams). The frequency of standing sound waves (p-modes) is labeled as ω_p . The forcing amplitude is $f_0 = 0.01$.

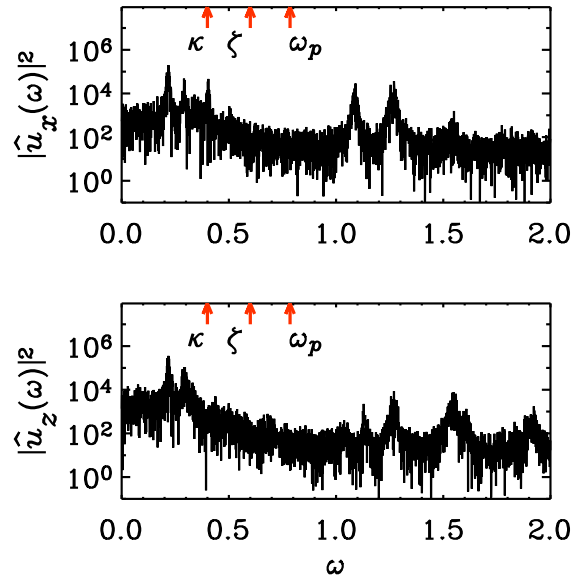


Fig. 6. Same as Fig. 5, but without initial velocity perturbation corresponding to a perfectly circular orbit. Note that the lower beat frequency, $\omega_1 = \zeta - \kappa = 0.2$, appears to be excited in both horizontal and vertical velocity components, while the upper beat frequency, $\omega_{11} = \zeta + \kappa = 1$, appears only in the radial velocity component.

However, it turned out that in the present case the initial perturbations drive epicyclic oscillations that, once excited, do not easily decay. In Fig. 4 we show the evolution of the radial and vertical velocity components at one point (u_x and u_z , respectively) in viscous units. Here the initial velocity perturbation was chosen to be $\mathbf{u} = (0.1, 0, 0.1)$. The initial x velocity is compatible with the shearing periodic boundary conditions, but a uniform vertical velocity is not. This turns out to be not a problem, because viscosity is able to damp the initially produced sharp gradients that occur near the boundary to satisfy $u_z = 0$.

Looking at Fig. 4 it is clear that there is hardly any decay. On the other hand, if no perturbation is applied initially, some oscillations are still being generated by the turbulence, as can be seen from the temporal Fourier spectra of the radial and vertical velocity components at one point in the domain, $|\hat{u}_x(\omega)|^2$ and $|\hat{u}_z(\omega)|^2$, respectively. These are shown in Fig. 5 and Fig. 6 for the cases with and without initial perturbations that would initialize epicyclic oscillations.

Indeed, in Fig. 5 one sees quite clearly the radial epicyclic frequency $\kappa = 0.4$ in the radial velocity component and the vertical epicyclic frequency $\zeta = 0.6$ in the vertical velocity component. However, the latter seems to be shifted toward a somewhat higher frequency (about 0.7), which might be due to the interaction with the vertical p-mode frequency, $\omega_p = c_s\pi/L_z \approx 0.78$.

It turns out that even when the oscillations are not present initially, some discrete frequencies are still being excited that lie near the lower and upper beat frequencies ($\omega_1 = \zeta - \kappa = 0.2$ and $\omega_{11} = \zeta + \kappa = 1$; see Fig. 6). However, the match is only approximate, suggesting that the cause of the additional

² <http://www.nordita.dk/software/pencil-code>

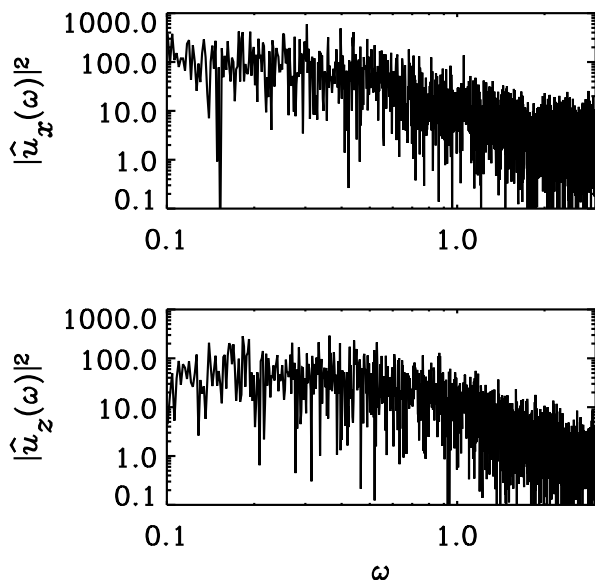


Fig. 7. Same as Fig. 5, but with magnetic field and no forcing, and in double-logarithmic representation. Thus, turbulence is generated by the MRI. As in Fig. 5, an initial perturbation of amplitude 0.1 has been applied. Note that for low frequencies the spectrum is nearly flat and lacks any discrete frequencies.

peaks in the spectra might not necessarily be related to beat phenomena.

It is plausible that epicyclic oscillations in discs can be excited stochastically. This is analogous to the excitations of p-modes in the sun and in stars (Goldreich & Kumar 1990). Similar arguments may also be applied to discs in order to explain the quasiperiodic oscillations (QPOs) in terms of resonances between different vertical and horizontal epicyclic frequencies (Abramowicz et al. 2003a,b, Kato 2004, Kluźniak et al. 2004, Lee et al. 2004).

Next we compare with a case where magnetic fields are included so that turbulence can be produced as a result of the MRI. No forcing function is therefore applied in the momentum equation. It turns out that in this case the power spectrum is more nearly flat and does not show discrete frequencies as in the purely hydrodynamic cases with an explicit forcing function; see Fig. 7.

The absence of discrete frequencies in the velocity power spectrum of MRI-driven turbulence is surprising. In order to inspect further what happens after the initial kick that was imposed via the initial condition, we plot in Fig. 8 the time evolution for all three runs during the first 300 time units. (The total duration of these runs is around 10,000 time units.) It is clear from the figure that in the case of forced turbulence the amplitude of the epicycles remains dominant. In the case of MRI-driven turbulence, the epicycles are essentially swamped by the comparatively strong level of turbulence. By comparison, in the nonmagnetic case of forced turbulence some systematic oscillation pattern is visible even when there is no initial perturbation giving rise to epicycles.

Finally, we present a case where the shear parameter q is chosen to be 1.85, so the radial epicyclic frequency is now different from the rotation frequency, i.e. $\kappa = 0.22$, while

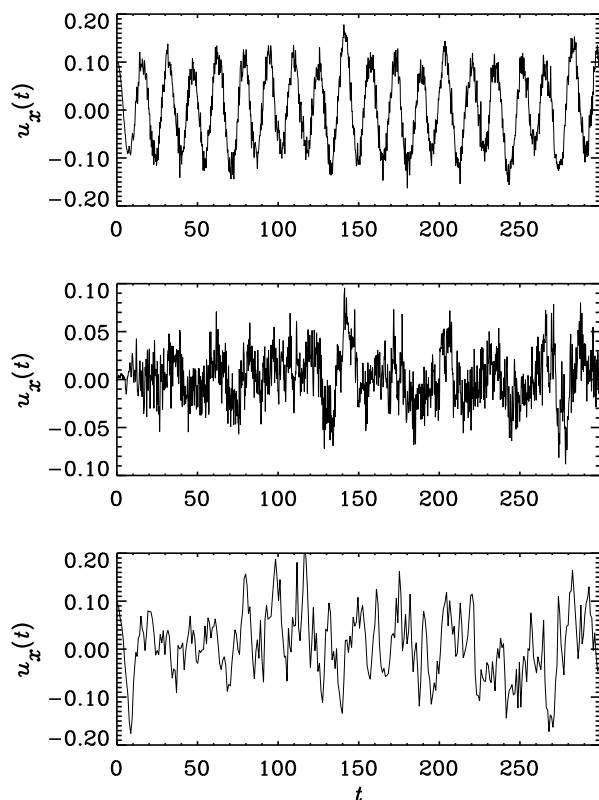


Fig. 8. Comparison of the time series for the runs shown in Figs 5–7. Only the beginning of the time series are shown. Note that in the last panel the MRI driven turbulence quickly wipes out the initial perturbation and no epicyclic oscillations are visible.

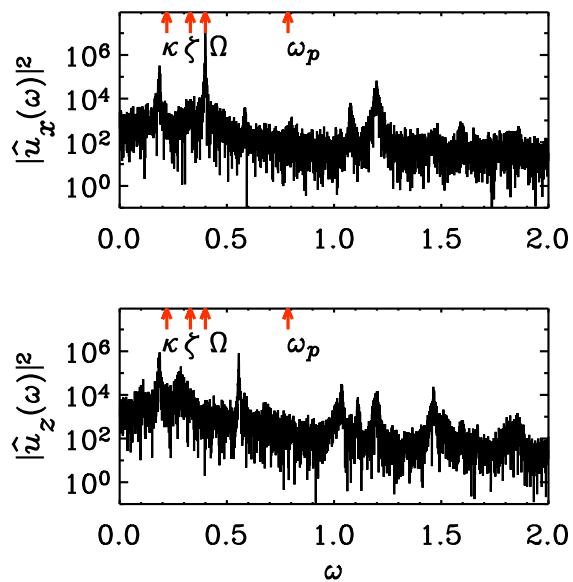


Fig. 9. Same as Fig. 5, but $\kappa = 0.22$, $\zeta = 0.33 \approx \frac{3}{2}\kappa$, and $\Omega = 0.4$.

$\Omega = 0.4$. The vertical epicyclic frequency is chosen to be $\zeta = 0.33 \approx \frac{3}{2}\kappa$. It turns out that there is still a pronounced peak at $0.4 (= \Omega)$, while some of the earlier detected frequencies (0.2 and 1.0), which are still present, lost their originally anticipated interpretation; see Fig. 9. The vertical ve-

locity has no longer a peak at $\zeta = 0.33$, but instead at a higher frequency of about 0.5. However, it appears still possible to interpret this as some interplay between $\zeta = 0.33$ and $\omega_p = 0.78$. The frequency 0.2 is still visible in the spectra, but with the new values of κ and ζ it is no longer possible to explain this as the lower beat frequency between the two. Although this result is perhaps somewhat disappointing in terms of interpreting QPOs, these experiments highlight the general usefulness of using the shearing sheet approximation which allows these kinds of experiments to be carried out without difficulties.

The above discussion is interesting in its own right and deserves certainly more attention. However, this method is obviously not well suited for determining turbulent transport coefficients. Therefore we now describe another method that has recently been developed in the hydromagnetic context for determining dynamo parameters.

5. Tensorial turbulent resistivity

The theory of turbulent resistivity is in many ways more developed than the theory of turbulent viscosity. In dynamo theory it has recently become possible to determine quite accurately not only the turbulent resistivity, but also its full tensorial form and other components that can be non-dissipative and hence important for dynamo action. While in the hydrodynamic case one is interested in the correlation $\overline{u_i u_j}$, one is here interested in the correlation $\overline{u_j b_j}$, or more specifically in the electromotive force $\overline{\mathcal{E}}_i = \epsilon_{ijk} \overline{u_j b_k}$. Assuming that the mean field is spatially smooth (which may not be the case in practice) one can truncate the expression for $\overline{\mathcal{E}}_i$ in terms of \overline{B}_j and its derivatives after the first derivative, so one has

$$\overline{\mathcal{E}}_i = \alpha_{ij} \overline{B}_j + \eta_{ijk} \overline{B}_{j,k}. \quad (22)$$

The components of α_{ij} tensor are usually quite easily determined from simulations by imposing a uniform magnetic field \overline{B}_j and measuring the resulting electromotive force $\overline{\mathcal{E}}_i$, so that $\alpha_{ij} = \overline{\mathcal{E}}_i / \overline{B}_j$ is obtained straightforwardly. The reason this works is because for a uniform field all derivatives of \overline{B}_j vanish, so there are no higher order terms. Calculating the components of η_{ijk} is usually harder, especially when the mean field may no longer be smooth and its derivatives may vanish in places. A method that has been used for accretion disc turbulence is based on a fitting procedure of the measured mean field and the mean electromotive force to Eq. (22) by calculating moments of the form $\langle \overline{\mathcal{E}}_i \overline{B}_j \rangle$, $\langle \overline{\mathcal{E}}_i \overline{B}_{j,k} \rangle$, as well as $\langle \overline{B}_i \overline{B}_j \rangle$ and $\langle \overline{B}_i \overline{B}_{j,k} \rangle$ (Brandenburg & Sokoloff 2002, Kowal et al. 2005).

A general procedure for determining the full α_{ij} and η_{ijk} tensors from a simulation is to calculate the electromotive force after applying test fields of different directions and with different gradients (Schinnerer et al. 2005). In the following we adopt xy averages, so the resulting mean fields depend only on z and t , and only \overline{B}_x and \overline{B}_y are non-trivial ($\overline{B}_z = 0$ because of the solenoidality $\overline{\mathbf{B}}$). Therefore, only the four components of α_{ij} and the four components of η_{ij3} with $i, j = 1, 2$ are non-trivial. Here, the numbers 1, 2, 3 refer to the cartesian x, y, z components.

In the present case of one-dimensional mean fields it is advantageous to rewrite Eq. (22) in the form

$$\overline{\mathcal{E}}_i = \alpha_{ij} \overline{B}_j - \tilde{\eta}_{ij} \overline{J}_j, \quad i, j = 1, 2, \quad (23)$$

where $\overline{\mathbf{J}} = \nabla \times \overline{\mathbf{B}}$ is the mean current density, and

$$\tilde{\eta}_{il} = \eta_{ijk} \epsilon_{jkl} \quad (24)$$

is the resistivity tensor operating only on the mean current density. In the special case of one-dimensional averages there is no extra information contained in the symmetric part of the $\overline{B}_{j,k}$ tensor that is not already contained in the components of $\overline{\mathbf{J}}$. In fact, the four components of η_{ij3} map uniquely to those of $\tilde{\eta}_{il}$ via

$$\begin{pmatrix} \tilde{\eta}_{11} & \tilde{\eta}_{12} \\ \tilde{\eta}_{21} & \tilde{\eta}_{22} \end{pmatrix} = \begin{pmatrix} \eta_{123} & -\eta_{113} \\ \eta_{223} & -\eta_{213} \end{pmatrix}. \quad (25)$$

This fact was also used in Brandenburg & Sokoloff (2002). The diagonal components of $\tilde{\eta}_{ij}$ correspond to turbulent resistivity, while its off-diagonal components can be responsible for driving dynamo action [$\Omega \times \overline{\mathbf{J}}$ and $\overline{\mathbf{W}} \times \overline{\mathbf{J}}$ effects; see, Rädler (1969) and Rogachevskii & Kleeorin (2003, 2004), Rädler & Stepanov (2005)]. Conversely, the diagonal components of the α tensor can be responsible for dynamo action while the off-diagonal components are responsible for non-regenerative turbulent pumping effects (Krause & Rädler 1980). It should be noted, however, that for linear shear flows Rüdiger & Kitchatinov (2005) find that the signs of the relevant coefficients of $\tilde{\eta}_{ij}$ are such that dynamo action is not possible for small magnetic Prandtl numbers.

In summary, in the present case of one-dimensional mean fields, $\overline{\mathbf{B}} = \overline{\mathbf{B}}(z, t)$, there are altogether 4 + 4 unknowns. The idea is to calculate the electromotive force

$$\overline{\mathcal{E}}^{(p,q)} = \overline{\mathbf{u}} \times \mathbf{b}^{(p,q)} \quad (26)$$

for the excess magnetic fluctuations, $\mathbf{b}^{(p,q)}$, that are due to a given test field $\overline{\mathbf{B}}^{(p,q)}$, where the labels p and q characterize the test field (p gives its nonvanishing component and $q = 1$ or 2 stands for cosine or sine-like test fields). The calculation of the electromotive force requires solving simultaneously a set of equations of the form

$$\frac{\partial \mathbf{b}^{(p,q)}}{\partial t} = \nabla \times [(\overline{\mathbf{U}} + \mathbf{u}) \times \overline{\mathbf{B}}^{(p,q)}] + \eta \nabla^2 \mathbf{b}^{(p,q)} + \mathbf{G} \quad (27)$$

for each test field $\overline{\mathbf{B}}^{(p,q)}$. Here, $\mathbf{G} = \nabla \times [\mathbf{u} \times \mathbf{b}^{(p,q)} - \mathbf{u} \times \overline{\mathbf{b}}^{(p,q)}]$ is a term nonlinear in the fluctuation. This term would be ignored in the first order smoothing approximation, but it can be kept in a simulation if desired. (In the present considerations it is neglected.)

The four test fields considered in the present problem of one-dimensional mean fields are

$$\overline{\mathbf{B}}^{(1,1)} = \begin{pmatrix} \cos k_1 z \\ 0 \\ 0 \end{pmatrix}, \quad \overline{\mathbf{B}}^{(1,2)} = \begin{pmatrix} \sin k_1 z \\ 0 \\ 0 \end{pmatrix}, \quad (28)$$

$$\overline{\mathbf{B}}^{(2,1)} = \begin{pmatrix} 0 \\ \cos k_1 z \\ 0 \end{pmatrix}, \quad \overline{\mathbf{B}}^{(2,2)} = \begin{pmatrix} 0 \\ \sin k_1 z \\ 0 \end{pmatrix}. \quad (29)$$

As an example, consider the x component of $\overline{\mathcal{E}}^{(p,q)}$ for $p = 1$ and both values of q ,

$$\overline{\mathcal{E}}_1^{(1,1)} = \alpha_{11} \cos k_1 z - \eta_{113} \sin k_1 z, \quad (30)$$

$$\overline{\mathcal{E}}_1^{(1,2)} = \alpha_{11} \sin k_1 z + \eta_{113} \cos k_1 z. \quad (31)$$

For $p = 2$, and/or for $i = 2$, one obtains a similar pair of equations with the same arrangement of cosine and sine functions. So, for each of the four combinations of i and j ($= p$) the set of two coefficient, α_{ij} and η_{ij3} , is obtained as

$$\begin{pmatrix} \alpha_{ij} \\ \eta_{ij3} \end{pmatrix} = \mathbf{M}^{-1} \begin{pmatrix} \overline{\mathcal{E}}_i^{(j,1)} \\ \overline{\mathcal{E}}_i^{(j,2)} \end{pmatrix}, \quad (32)$$

where the matrix

$$\mathbf{M} = \begin{pmatrix} \cos k_1 z & -\sin k_1 z \\ \sin k_1 z & \cos k_1 z \end{pmatrix} \quad (33)$$

is the same for each value of p and each of the two components $i = 1, 2$ of $\overline{\mathcal{E}}_i^{(p,q)}$. Finally, $\tilde{\eta}$ is calculated using Eq. (24). Note that $\det \mathbf{M} = 1$, so the inversion procedure is well behaved and even trivial.

The test field algorithm described above has been implemented in the PENCIL CODE. The results are shown in Fig. 10 for the case of forced turbulence and in Fig. 11 for the case of MRI-driven turbulence. We recall that in both cases the effect of stratification is included.

The following main results can be summarized from this analysis. First, for forced turbulence the α effect (especially the yy component that is relevant for acting on the already strong toroidal \overline{B}_y field) is *positive* in the northern hemisphere $z > 0$ [as expected for cyclonic and anti-cyclonic events; see Parker (1979) and Krause & Rädler (1980)]. However, in the case of MRI-driven turbulence the sign of α_{yy} is reversed, confirming the early results of Brandenburg et al. (1995). This may be explained in terms of strong flux tubes that are buoyant and therefore rising, but that also exhibit a converging flow from the $\mathbf{B} \cdot \nabla \mathbf{B}$ tension force that points toward to strongest parts of the tube (Brandenburg 1998). The same result has been obtained by Rüdiger & Pipin (2000) for magnetically driven turbulence using first order smoothing. Their result is specifically due to the dominance of the current helicity term and is not connected with the buoyancy term (Blackman 2005).

Second, the off-diagonal components of the α tensor are such that they correspond to a turbulent pumping effect, $\overline{\mathcal{E}} = \dots + \gamma \times \overline{\mathbf{B}}$, where $\gamma_z = \frac{1}{2}(\alpha_{yx} - \alpha_{xy})$. Theoretically the pumping velocity is expected to be in the direction of negative turbulent intensity (Roberts & Soward 1975). In the present case of forced turbulence the rms velocity is approximately independent of height, but the density decreases outwards, causing therefore an outward turbulent pumping effect (second panel of Fig. 10). For MRI-driven turbulence, the density also decreases outward, but the rms velocity increases as the density decreases such that $\overline{\rho \mathbf{u}^2}$ is approximately constant. This may be the reason for not having much of a vertical turbulent pumping effect in MRI-driven turbulence.

Third, the two diagonal components of $\tilde{\eta}_{ij}$ are in both cases positive (i.e. indeed diffusive, which is non-trivial!) and the two components, $\tilde{\eta}_{xx}$ and $\tilde{\eta}_{yy}$, are almost equally big. [We

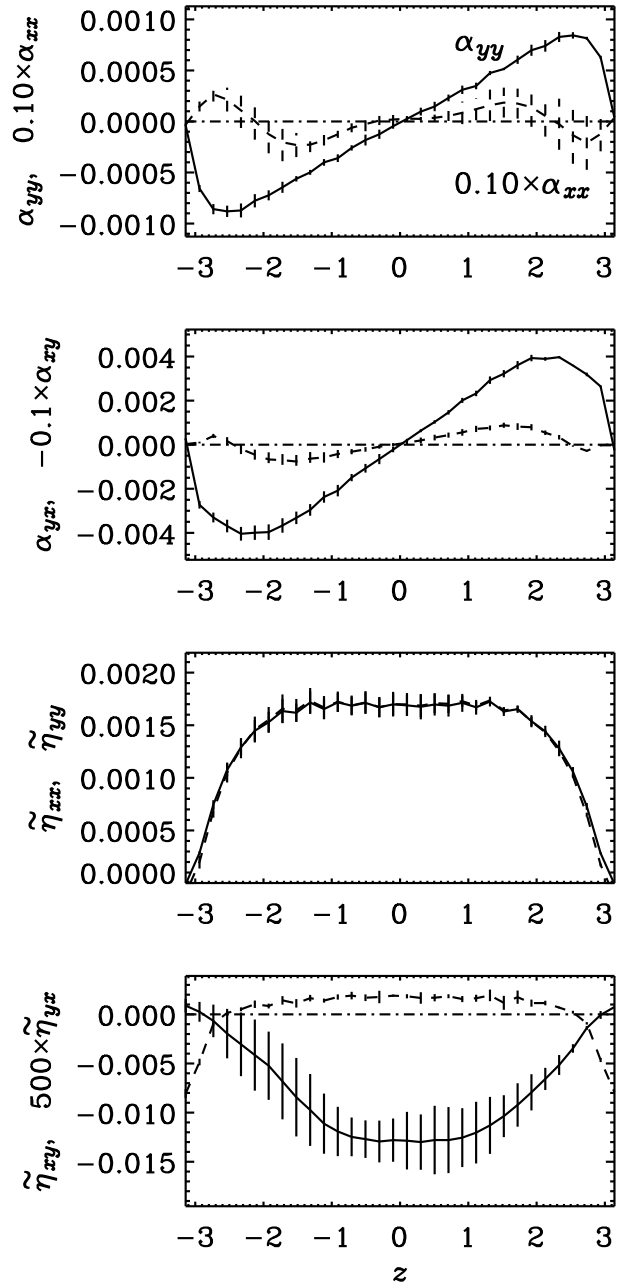


Fig. 10. Magnetic turbulent transport coefficients for forced turbulence. Solid and dashed lines refer respectively to the first and second quantity denoted on the corresponding axis. The error bars have been obtained by calculating the maximum departure over the three possibilities obtained by considering only 1/3 of the full time series.

recall that in Brandenburg & Sokoloff (2002) it was found that $\tilde{\eta}_{yy}$ (responsible for diffusion of \overline{B}_x) was very small, but this result was perhaps not accurate.]

Fourth, the signs of the off-diagonal components of $\tilde{\eta}_{ij}$ are here such that they would not correspond to a dynamo effect of the form $\overline{\mathcal{E}} = \dots + \delta \times \overline{\mathbf{J}}$, where $\delta_z = \frac{1}{2}(\tilde{\eta}_{xy} - \tilde{\eta}_{yx})$. Growing solutions require that the product of shear (here $S = -\frac{3}{2}\Omega$) and δ_z is negative (Brandenburg & Subramanian 2005a,b). However, since $\delta_z < 0$ for forced turbulence (Fig. 10), only decaying solutions are possible. This is in agreement with predictions by Rüdiger & Kitchatinov

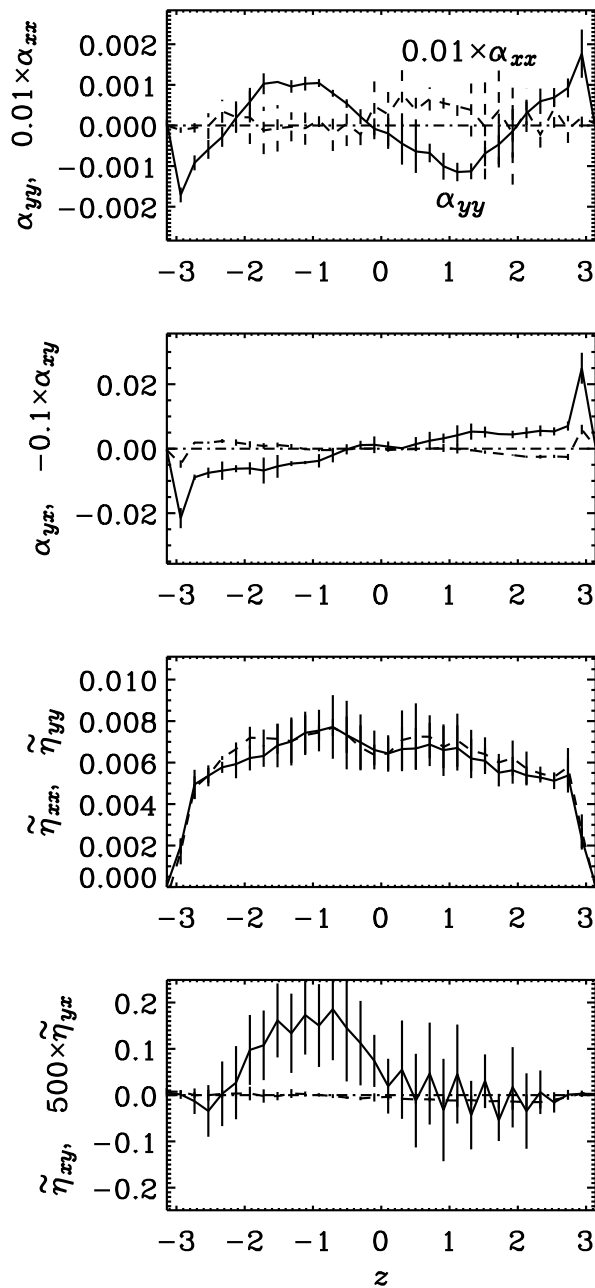


Fig. 11. Same as Fig. 10, but for MRI-driven turbulence.

(2005). For MRI-driven turbulence δ_z is within error bars either compatible with zero or positive in a few places. Thus, the $\overline{\mathbf{W}} \times \overline{\mathbf{J}}$ effect is perhaps possible here. However, for the full 2×2 tensor, $\tilde{\eta}_{ij}$, it is important to consider its tensorial nature. It turns out that a necessary condition for dynamo action is

$$\tilde{\eta}_{yx} k_z^2 (\tilde{\eta}_{xy} k_z^2 + S) > 0 \quad (\text{for dynamo action}), \quad (34)$$

so the sign of $\tilde{\eta}_{yx}$ is now crucial; see Appendix B for details. Even then the simulations would not suggest dynamo action from the $\overline{\mathbf{W}} \times \overline{\mathbf{J}}$ effect. In any case, it is important to consider simulations with larger magnetic Reynolds. So far there is only the example of solar-like shear flow turbulence of Brandenburg (2005) where the $\overline{\mathbf{W}} \times \overline{\mathbf{J}}$ effect is a leading

candidate for explaining the generation of large scale fields in the absence of helicity.

6. Conclusions

The present investigations have demonstrated a number of new and previously unknown properties both for forced and MRI-driven turbulence in the shearing box approximation. In many respects these two cases are quite different. First of all, the fact that for MRI-driven turbulence most of the dissipation happens near the upper and lower boundaries of the disc (i.e. in the disc corona) is peculiar to this case and is not in general true. Indeed, for non-magnetic discs most of the dissipation is expected near the midplane where the density is largest. Without entering the discussion about the reality of non-magnetic turbulence in accretion discs (e.g. Balbus et al. 1996), we note that under some circumstances (e.g. in protostellar discs where the electric conductivity is poor) the MRI is not likely to operate, so less efficient mechanisms such as the inflow into the disc during its formation and vertical shear (Urpin & Brandenburg 1998) cannot be excluded as possible agents facilitating turbulence. Also the possibility of nonlinear instabilities (Richard & Zahn 1999, Chagelishvili et al. 2003, Afshordi et al. 2005) should be mentioned. In any case, comparing magnetic and non-magnetic cases is important in order to assess the potential validity of general turbulence concepts that have mainly been studied under forced non-magnetic conditions.

There are a number of alternative ways of determining the turbulent viscosity in discs. Three methods have already been compared in the context of MRI-driven turbulence by determining the stress either explicitly, from the heating rate, or from the radial mass accretion rate (Brandenburg et al. 1996a). A rather obvious alternative is to consider the decay of an initial wave-like perturbation and to measure the decay of this signal. Although this method gives sensible results in the context of non-shearing and non-rotating flows (Yousef et al. 2003), in the present case it cannot be used for this purpose, because epicyclic oscillations are being initialized that hardly decay. In fact, at least in the hydrodynamic case with not too strong forcing there is clear evidence that epicyclic oscillations can actually be excited stochastically—very much like the p-modes in the sun. This may be important for understanding the quasi-periodic oscillations discovered recently in some pulsars (e.g., Lee et al. 2004), and in particular the connection with the possibility of exciting resonances at the beat frequencies for non-equal vertical and radial epicyclic frequencies.

Given that the turbulence is in general non-isotropic (owing to shear and rotation, as well as stratification), the turbulent transport coefficients are in general also non-isotropic. For practical calculations of toroidally averaged accretion flows (e.g., Kley et al. 1993, Igumenshchev et al. 1996) it is therefore essential to know the full tensorial structure as well as other possibly non-diffusive contributions. Significant progress has been made in determining the full tensorial structure of the turbulent resistivity and alpha effect. Somewhat surprisingly, it turned out that the two diagonal compo-

nents of the resistivity tensor are nearly equal. Furthermore, in the non-MRI case the off-diagonal components can even give rise to dynamo action (the so-called $\overline{\mathbf{W}} \times \overline{\mathbf{J}}$ or shear-current effect). As far as the α effect is concerned, an earlier result about the different signs for MRI and forced turbulence is confirmed.

Similar investigations can probably also be carried out for determining the tensorial nature of turbulent viscosity and possibly other non-diffusive effects that are known in other circumstances (e.g., Rüdiger & Hollerbach 2004). Most important is perhaps the investigation of stochastically excited epicyclic oscillations in connection with the kilohertz quasiperiodic oscillations found in some pulsars. Obviously, more systematic investigations should be carried out to determine the dependence on forcing amplitude of the turbulence and to check whether similar oscillations are also possible for MRI-driven turbulence.

Acknowledgements. I thank Eric G. Blackman, Günther Rüdiger, and Kandaswamy Subramanian for suggestions and comments on the manuscript, and Karl-Heinz Rädler and Martin Schrunner for collaborating with me on the implementation and testing of the technique described in Sect. 5. The Danish Center for Scientific Computing is acknowledged for granting time on the Horseshoe cluster.

References

- Abramowicz, M. A., Bulik, T., Bursa, M., Kluźniak, W.: 2003a, *A&A* 404, L21
- Abramowicz, M. A., Karas, V., Kluźniak, W., Lee, W. H., Rebusco, P.: 2003b, *PASJ* 55, 467
- Afshordi, N., Mukhopadhyay, B., Narayan, R.: 2005, *ApJ* 629, 373
- Arlt R., Rüdiger G.: 2001, *A&A* 374, 1035
- Balbus, S. A.: 2004, *ApJ* 600, 865
- Balbus, S. A. Hawley, J. F.: 1991, *ApJ* 376, 214
- Balbus, S. A. Hawley, J. F.: 1998, *ReMP* 70, 1
- Balbus, S. A., Papaloizou, J. C. B.: 1999, *ApJ* 521, 650
- Balbus, S. A., Hawley, J. F., Stone, J. M.: 1996, *ApJ* 467, 76
- Blackman, E. G.: 2005, personal communication
- Brandenburg, A.: 1998, in M. A. Abramowicz, G. Björnsson, J. E. Pringle (eds.), *Theory of Black Hole Accretion Discs*, Cambridge University Press, Cambridge, p. 61
- Brandenburg, A.: 2001, *ApJ* 550, 824 (B01)
- Brandenburg, A.: 2003, in A. Ferriz-Mas, M. Núñez (eds.), *Advances in nonlinear dynamos*, Taylor & Francis, London, p. 269
- Brandenburg, A.: 2005, *ApJ* 625, 539
- Brandenburg, A., Sokoloff, D.: 2002, *GApFD* 96, 319
- Brandenburg, A., Subramanian, K.: 2005a, *AN* 326, 400
- Brandenburg, A., Subramanian, K.: 2005b, *PhR* 417, 1
- Brandenburg, A., Nordlund, Å., Stein, R. F., Torkelsson, U.: 1995, *ApJ* 446, 741
- Brandenburg, A., Nordlund, Å., Stein, R. F., Torkelsson, U.: 1996a, *ApJ* 458, L45
- Brandenburg, A., Nordlund, Å., Stein, R. F., Torkelsson, U.: 1996b, in S. Kato, S. Inagaki, S. Mineshige, J. Fukue (eds.), *Physics of Accretion Discs*, Gordon and Breach Science Publishers, p. 285
- Brandenburg, A., Dintrans, B., Haugen, N. E. L.: 2004, in R. Rosner, G. Rüdiger, A. Bonanno (eds.), *MHD Couette flows: experiments and models*, AIP Conf. Proc. **733**, p. 122
- Carballido, A., Stone, J. M., Pringle, J. E.: 2005, *MNRAS* 358, 1055
- Chagelishvili, G. D., Zahn, J.-P., Tevzadze, A. G., Lominadze, J. G.: 2003, *A&A* 402, 401
- De Villiers, J.-P., Hawley, J. F.: 2003, *ApJ* 592, 1060
- Frank, J., King, A. R., & Raine, D. J.: 1992, *Accretion power in astrophysics* (Cambridge University Press, Cambridge)
- Goldreich, P., Kumar, P.: 1990, *ApJ* 363, 694
- Hawley, J. F., Gammie, C. F., Balbus, S. A.: 1995, *ApJ* 440, 742
- Hawley, J. F., Gammie, C. F., Balbus, S. A.: 1996, *ApJ* 464, 690
- Hawley, J. F.: 2000, *ApJ* 528, 462
- Igumenshchev, I. V., Chen, X., Abramowicz, M. A.: 1996, *MNRAS* 278, 236
- Johansen, A., Klahr, H.: 2005, *ApJ* (in press) (arXiv: astro-ph/0501641)
- Kato, Y.: 2004, *PASJ* 56, 931
- Kley, W., Papaloizou, J. C. B., Lin, D. N. C.: 1993, *ApJ* 409, 739
- Kowal, G., Otmianowska-Mazur, K., Hanasz, M.: 2005, in K.T. Chyży, K. Otmianowska-Mazur, M. Soida, and R.-J. Dettmar (eds.), *The magnetized plasma in galaxy evolution*, Jagiellonian University, p. 171
- Kluźniak, W., Abramowicz, M. A., Kato, S., Lee, W. H., Stergioulas, N.: 2004, *ApJ* 603, L89
- Krause, F., Rädler, K.-H.: 1980, *Mean-Field Magnetohydrodynamics and Dynamo Theory* (Pergamon Press, Oxford)
- Lee, W. H., Abramowicz, M. A., Kluźniak, W.: 2004, *ApJ* 603, L93
- Matsumoto, R., Tajima, T.: 1995, *ApJ* 445, 767
- Parker, E. N.: 1979, *Cosmical Magnetic Fields* (Clarendon Press, Oxford)
- Rädler, K.-H.: 1969, *Geod. Geophys. Veröff.*, Reihe II 13, 131
- Rädler, K.-H., Stepanov, R.: 2005, *JFM* (submitted)
- Richard, D., Zahn, J.-P.: 1999, *A&A* 347, 734
- Roberts, P. H., Soward, A. M.: 1975, *AN* 296, 49
- Rogachevskii, I., Kleeorin, N.: 2003, *PhRvE* 68, 036301
- Rogachevskii, I., Kleeorin, N.: 2004, *PhRvE* 70, 046310
- Rüdiger, G.: 1987, *AcA* 37, 223
- Rüdiger, G., Pipin, V. V.: 2000, *A&A* 362, 756
- Rüdiger, G., Hollerbach, R.: 2004, *The magnetic universe* (Wiley-VCH, Weinheim)
- Rüdiger, G., Kitchatinov, L. L.: 2005, *PhRvE*, submitted
- Schrinner, M., Rädler, K.-H., Schmitt, D., Rheinhardt, M., Christensen, U.: 2005, *AN* 326, 245
- Shakura, N. I., Sunyaev, R. A.: 1973, *A&A* 24, 337
- Stone, J. M., Hawley, J. F., Gammie, C. F., Balbus, S. A.: 1996, *ApJ* 463, 656
- Torkelsson, U., Ogilvie, G. I., Brandenburg, A., Pringle, J. E., Nordlund, Å., & Stein, R. F.: 2000, *MNRAS* 318, 47
- Turner, N. J.: 2004, *ApJ* 605, L45
- Urpin, V., Brandenburg, A.: 1998, *MNRAS* 294, 399
- Yousef, T. A., Brandenburg, A., Rüdiger, G.: 2003, *A&A* 411, 321

Appendix A: The forcing function

For completeness we specify here the forcing function used in the present paper³. It is defined as

$$\mathbf{f}(\mathbf{x}, t) = \text{Re}\{N\mathbf{f}_{\mathbf{k}(t)} \exp[i\mathbf{k}(t) \cdot \mathbf{x} + i\phi(t)]\}, \quad (\text{A1})$$

where \mathbf{x} is the position vector. The wavevector $\mathbf{k}(t)$ and the random phase $-\pi < \phi(t) \leq \pi$ change at every time step, so $\mathbf{f}(\mathbf{x}, t)$ is δ -correlated in time. For the time-integrated forcing function to be independent of the length of the time step δt , the normalization factor N has to be proportional to $\delta t^{-1/2}$. On dimensional grounds it is chosen to be $N = f_0 c_s (|\mathbf{k}| c_s / \delta t)^{1/2}$, where f_0 is a nondimensional forcing amplitude. The value of the coefficient f_0 is chosen such that the maximum Mach number stays below about 0.5; in practice this means $f_0 = 0.01 \dots 0.05$, depending on the average

³ This forcing function was also used by Brandenburg (2001), but in his Eq. (5) the factor 2 in the denominator should have been replaced by $\sqrt{2}$ for a proper normalization.

forcing wavenumber. At each timestep we select randomly one of many possible wavevectors in a certain range around a given forcing wavenumber. The average wavenumber is referred to as k_f . Two different wavenumber intervals are considered: 1...2 for $k_f = 1.5$ and 4.5...5.5 for $k_f = 5$. We force the system with transverse helical waves,

$$\mathbf{f}_{\mathbf{k}} = (\mathbf{k} \times \hat{\mathbf{e}}) / \sqrt{\mathbf{k}^2 - (\mathbf{k} \cdot \hat{\mathbf{e}})^2}, \quad (\text{A2})$$

where $\hat{\mathbf{e}}$ is an arbitrary unit vector not aligned with \mathbf{k} ; note that $|\mathbf{f}_{\mathbf{k}}|^2 = 1$.

Appendix B: Dispersion relation for tensorial $\tilde{\eta}$

The dispersion relation for the dynamo problem with δ effect is (Brandenburg & Subramanian 2005)

$$\lambda_{\pm} = -\eta_{\text{T}} k^2 \pm \sqrt{-(\mathbf{k} \cdot \boldsymbol{\delta})^2 k^2 - (\mathbf{k} \cdot \boldsymbol{\delta}) S k_z}, \quad (\text{B1})$$

where λ is the growth rate, k_x and k_z are the wavenumbers in the x and z directions, $\mathbf{k}^2 = k_x^2 + k_z^2$, and $\eta_{\text{T}} = \eta + \eta_t$ the sum of microscopic and turbulent diffusion.

We now consider the one-dimensional problem ($k_x = 0$) and treat all four components of $\tilde{\eta}_{ij}$ as independent, so we have the following set of two partial differential equations,

$$\dot{\overline{B}}_x = (\eta + \tilde{\eta}_{yy}) \overline{B}_x'' - \tilde{\eta}_{yx} \overline{B}_y'', \quad (\text{B2})$$

$$\dot{\overline{B}}_y = (\eta + \tilde{\eta}_{xx}) \overline{B}_y'' - \tilde{\eta}_{xy} \overline{B}_x'' + S \overline{B}_x, \quad (\text{B3})$$

where $S = -\frac{3}{2}\Omega$ is the shear coefficient. Using the abbreviation $n_{ij} = (\eta \delta_{ij} + \tilde{\eta}_{ij}) k_z^2$, this leads to the dispersion relation

$$\lambda_{\pm} = -\frac{1}{2}(n_{xx} + n_{yy}) \pm \sqrt{\frac{1}{4}(n_{xx} - n_{yy})^2 + n_{yx}(n_{xy} + S)}, \quad (\text{B4})$$

which reduces to the one-dimensional form of Eq. (B1) when $\tilde{\eta}_{xx} = \tilde{\eta}_{yy} = \eta_t$ and $\tilde{\eta}_{xy} = -\tilde{\eta}_{yx} = \delta$.